



ARTICLE

# A Connectivity Model for the Numerical Simulation of Microgel Flooding in Low-Permeability Reservoirs

Tao Wang<sup>1,2</sup>, Haiyang Yu<sup>1,\*</sup>, Jie Gao<sup>2</sup>, Fei Wang<sup>2</sup>, Xinlong Zhang<sup>3,\*</sup>, Hao Yang<sup>2</sup>, Guirong Di<sup>2</sup> and Pengrun Wang<sup>2</sup>

<sup>1</sup>State Key Laboratory of Petroleum Resources and Prospecting, China University of Petroleum-Beijing, Beijing, 102249, China

<sup>2</sup>China Oilfield Service Limited Production Optimization R&D Institute, Tianjin, 300459, China

<sup>3</sup>School of Petroleum Engineering, Yangtze University, Wuhan, 430100, China

\*Corresponding Authors: Haiyang Yu. Email: haiyangyu.cup@139.com; Xinlong Zhang. Email: zxinlong2022@163.com

Received: 23 September 2024; Accepted: 06 February 2025; Published: 30 May 2025

**ABSTRACT:** Oilfields worldwide are increasingly grappling with challenges such as early water breakthrough and high water production, yet direct, targeted solutions remain elusive. In recent years, chemical flooding techniques designed for tertiary oil recovery have garnered significant attention, with microgel flooding emerging as a particularly prominent area of research. Despite its promise, the complex mechanisms underlying microgel flooding have been rarely investigated numerically. This study aims to address these gaps by characterizing the distribution of microgel concentration and viscosity within different pore structures. To enhance the accuracy of these characterizations, the viscosity of microgels is adjusted to account for the shear effects induced by flow rate and the swelling effects driven by salinity variations. The absolute permeability of the rock and the relative permeability of both oil and microgel are also analyzed to elucidate the mechanisms of microgel flooding. Additionally, a connectivity model is employed to achieve a quantitative representation of fluid flow capacity. The proposed model is validated through conceptual examples and applied to real oilfield blocks, demonstrating its accuracy and practical applicability.

**KEYWORDS:** Connectivity model; chemical enhanced oil recovery; microgel flooding; numerical reservoir simulation; fractured reservoirs

## 1 Introduction

Oilfields encounter numerous challenges after entering high water-cut stage following extended periods of water injection. The water content of production wells in mature oilfields typically exceeds 90%, with annual declines in production making it increasingly difficult to maintain output through water injection [1]. However, a substantial amount of remaining oil in the reservoir remains inaccessible due to water flooding [2]. Statistics show that conventional water flooding usually leads to the recovery of only one-third to two-fifths oil from the geological reserves [3]. Therefore, replacing water flooding with advanced oilfield development technologies is a key approach for sustaining production in mature oilfields [4–7].

Enhanced oil recovery methods are employed to increase the production of hydrocarbon from reservoirs after primary and secondary recoveries. One of the successfully employed techniques is polymer flooding, which has shown significant improvements in both oil production and water management [8–11]. This technique is crucial for extracting trapped oil from mature oilfields, thereby increasing their effectiveness and lifespan. However, the effectiveness of polymer flooding in highly heterogeneous reservoirs



decreases during the mid-to-late stages of development. This decrease is due to reservoir heterogeneity and polymer retention, which can lead to “liquid absorption profile reversal.” This reversal hinders the effective production of medium- and low-permeability layers and limits the expansion of the swept volume, exacerbating interlayer conflicts and significantly reducing the efficiency of polymer flooding [12–14]. In response, microgel (also known as cross-linked polymer or movable gel) flooding has emerged as a novel technology for enhanced oil recovery.

Microgels demonstrated desirable performance in conformance control compared with uncrosslinked polymers and also showed to be a better candidate for in-depth penetration than polymers and bulk gels due to their viscoelastic properties [15]. Moreover, microgels do not have the disadvantages of pre-made gels, and the gelation parameter no longer an issue. Microgels can also be injected into the reservoir in formation water as a low-viscosity suspension. Most interestingly, microgels can selectively change the permeability, and the microgel selectively reduces the water permeability without reducing the oil permeability. Therefore, no occurrence of formation damage is expected, because their viscoelastic structure and flexibility allow oil to pass through low-permeability zones. Numerical modeling of polymer and gel propagation in porous media has been extensively studied to predict flow behavior, displacement efficiency, and interactions with reservoir heterogeneities [16–18]. However, there are many simulation parameters and complex calculations in polymer flooding, and it is difficult to balance simulation accuracy and speed in practical applications.

In this study, the concentration distribution of microgels in different pores was characterized to determine the particle phase separation and the corresponding viscosity distribution was determined. The viscosity of the microgel was corrected by considering the shear and swelling effect caused by the flow rate and salinity, respectively. The mechanism of microgel flooding was described by characterizing the absolute permeability of rock and the relative permeability of oil and microgel. Based on the connectivity model proposed by Zhao et al. [19], we characterize the dual-medium model considering the influence of cross-flow and realize the quantitative characterization of fluid flow capacity. By verifying the conceptual examples and applying actual blocks, the accuracy of the model proposed in this paper is verified, which can accurately reflect the mechanism of microgel flooding.

## 2 Characterization of the Oil Displacement Mechanism of Microgel-Based Chemical Agents

Microgels are excellent examples of acrylamide-based covalently cross-linked polymeric gels, with particle sizes varying between 0.3–2  $\mu\text{m}$ . When the particle size was less than 1  $\mu\text{m}$ , the concentration of the microgel solution in the pores of different sizes remained uniform due to Brownian motion. However, microgel particles tend to preferentially enter larger channels with lower resistance and higher flow rates, carried by the fluid. This causes the carrying fluid to enter smaller channels with lower flow rates, resulting in particle phase separation [20]. In other words, microgel agents can seal large pore channels while leaving smaller ones unsealed. Based on this property, Sun et al. [21] proposed a mathematical model for quantitatively calculating the microgel concentration distribution.

Assuming there are  $N$  outlets, the fractional flow of fluid through each outlet is expressed as follows:

$$x_i = \frac{q_i}{\sum_{i=1}^N q_i} \quad (1)$$

where  $x_i$  is the fractional flow rate at outlet  $i$ , uncaused, and  $q_i$  is the flow rate at outlet  $i$ ,  $\text{m}^3/\text{s}$ .

When the flow rate through an outlet is less than or equal to a certain value  $x_i^*$ , the microgel concentration in that channel is zero. This value  $x_i^*$  is then defined as the critical flow rate.

The concentration distribution of the microgel solution is expressed as follows:

$$\begin{cases} y_i(x_i) = 0 & x_i \leq x_i^* \\ y_i(x_i) = a + \frac{1-a}{Nx_i} & 1-x_i^* \geq x_i > x_i^* \\ y_i(x_i) = \frac{1}{x_i} & x_i > 1-x_i^* \end{cases} \quad (2)$$

where  $y_i$  is the concentration of the microgel solution,  $a$  is an experimentally determined parameter of the equation, and  $N$  is the number of connected channels.

Based on Thurston et al., defined the viscosity–concentration relationship for a microgel solution is expressed as follows [22]:

$$\mu_l = \mu_w (1 + ry_i + sy_i^2) \quad (3)$$

where  $\mu_l$  is the viscosity of the microgel solution,  $\mu_w$  is the viscosity of the aqueous phase,  $r$  and  $s$  are the experimentally determined model parameters, and  $y_i$  represents the concentration of the microgel solution, which is calculated using Eq. (2).

Under the influence of the flow rate, the viscosity of the microgels exhibits shear thinning, a stable state, and a shear thickening behavior in succession. In this study, we employed a hybrid rheological framework that combines the cross model for shear thinning behavior and a modified stress-dependent term to account for shear thickening at higher shear rates. To capture the continuous transition between these regimes, a blending function was used, ensuring that the model remained physically realistic and computationally stable at all shear rates. The viscosity is expressed as a function of shear rate:

$$\mu = \mu_l \left( 1 + \left( \frac{\gamma}{\gamma_c} \right)^n \right)^{-1} + \alpha \gamma^m \quad (4)$$

where  $\mu_l$  is the zero-shear viscosity,  $\gamma_c$  is the critical shear rate,  $n$  is the shear thinning index,  $\alpha$  is a proportionality constant, and  $m$  is the shear thickening index.

The swelling behavior of microgel particles is influenced by salt concentration and is modeled using the swelling ratio formula as follows:

$$Q = Q_0 (1 + k_s C_s)^{-1} \quad (5)$$

where  $Q_0$  is the swelling ratio in deionized water,  $C_s$  is the salinity concentration, and  $k_s$  is an empirically derived parameter that reflects salinity sensitivity.

The swelling of microgel particles, influenced by the ionic strength, is explicitly modeled. The swelling ratio ( $Q$ ) determines the effective particle volume fraction, which directly affects the viscosity:

$$\mu = \mu \left( \frac{\phi}{\phi_{\max}(C_s)} \right)^p \quad (6)$$

where  $\phi_{\max}$  is the salinity-dependent maximum packing fraction and  $p$  is a scaling exponent based on experimental data.

Multiple mechanisms influence reservoir fluid seepage after the injection of a microgel solution into the formation. The microgel solution alters the pore structure of rock, thereby affecting its absolute permeability.

However, the microgel solution interacts with crude oil, resulting in changes to the relative permeability of both the oil phase and the microgel.

Based on the theory proposed by Abdelgawad [23], the relationship between the absolute permeability reduction factor of the rock and the concentration of the microgel solution is given by the following:

$$R_k = 1 + \frac{b_k y_i}{1 + c_k y_i} (R_{k,\max} - 1) \quad (7)$$

where  $R_k$  is the absolute permeability decline coefficient of the rock,  $b_k$  and  $c_k$  are the experimentally determined coefficients of the equation, and  $R_{k,\max}$  is the maximum permeability decline coefficient.

The relative permeability of the oil phase to the microgel solution is expressed as follows:

$$k_{rp} = \frac{k_{rw}^0}{1 + a_{k1}X + a_{k2}X^2} \cdot \left( \frac{S_w - S_{wr}}{1 - S_{wr} - S_{or}} \right)^{ep1} \quad (8)$$

$$k_{ro} = \frac{k_{ro}^0}{1 + a_{k1}X} \cdot \left( \frac{S_w - S_{wr}}{1 - S_{wr} - S_{or}} \right)^{ep2} \quad (9)$$

where  $k_{ro}^0$  and  $k_{rw}^0$  are the relative permeability equation coefficients of the oil and water phases, respectively,  $S_w$  is water saturation,  $S_{wr}$  is bound water saturation,  $S_{or}$  is residual oil saturation,  $a_{k1}$  and  $a_{k2}$  are the experimentally measured equation parameters, and  $ep1$  and  $ep2$  are the experimentally measured equation indices.

### 3 Construction of Connectivity Model for Microgel Chemicals

The reservoir is discretized and simplified into a series of connected units, which are then used to establish material balance equations and perform pressure calculations. The inter-well connectivity model treats well sites as fundamental units and simplifies the complex geological description of the inter-well area into two key characteristic parameters, namely, inter-well conductivity and connectivity volume. The inter-well conductivity represents the seepage velocity per unit pressure difference, effectively reflecting the average seepage capacity and dominant conductivity direction between wells. The connectivity volume represents the material basis of the connectivity unit, indicating the range and volume of the inter-well water-drive control.

Assuming that  $i$  and  $j$  are oil recovery and water injection wells, respectively, the connected volume (Eq. (10)) and the connectivity conductivity (Eq. (11)) at the initial moment are calculated as follows:

$$V_{p,i,j}^0 = \frac{\bar{\phi}_{i,j} \bar{h}_{i,j} L_{i,j}}{\sum_{i=1}^{N_w-1} \left( \sum_{j=i+1}^{N_w} \bar{\phi}_{i,j} \bar{h}_{i,j} L_{i,j} \right)} V_R \quad (10)$$

$$T_{i,j}^0 = \alpha \frac{\bar{k}_{i,j} V_{p,i,j}^0}{\mu_0 \bar{\phi}_{i,j} L_{i,j}^2} \quad (11)$$

where  $\bar{\phi}_{i,j}$  is the arithmetic mean porosity between wells  $i$  and  $j$  at the initial moment,  $\bar{h}_{i,j}$  is the thickness between wells  $i$  and  $j$ ,  $\bar{k}_{i,j}$  is the permeability between wells  $i$  and  $j$  at the initial moment,  $L_{i,j}$  is the well spacing between wells  $i$  and  $j$ ,  $N_w$  is the total number of wells,  $\mu_0$  denotes the crude oil viscosity,  $V_R$  is the pore volume of the reservoir, and  $\alpha$  is the unit conversion factor.

If the concentration of the microgel solution in the connecting channel between wells  $i$  and  $j$  at a given moment is  $y_{ij}$ , the permeability decline factor  $R_{k,i,j}$  at that moment can be obtained according to Eq. (7) as follows:

$$R_{k,i,j} = 1 + \frac{b_k y_{ij}}{1 + c_k y_{ij}} (R_{k,\max} - 1) \quad (12)$$

Therefore, the permeability  $k_{a,i,j}$  of the connecting channel between wells  $i$  and  $j$  currently is

$$k_{a,i,j} = \left[ 1 + \frac{b_k y_{i,j}}{1 + c_k y_{ij}} (R_{k,\max} - 1) \right] \bar{k}_{i,j} \quad (13)$$

The fractured reservoir was modeled as a dual-medium system consisting of a matrix and fractures. The channeling effect between the fracture and matrix is considered, and separate material balance equations are established for the matrix and fracture systems. Since the microgel chemical agent is characterized by its ability to plug large pores while leaving smaller pores unobstructed, the microgel solution is directed exclusively into the fracture system and does not enter the matrix system. Therefore, permeability changes in the matrix system are not considered. Instead, only the permeability changes in the fracture system resulting from the injection of the microgel solution are characterized.

Thus, the material balance equations for the matrix and the fracture systems are expressed as follows:

$$\sum_{k=1}^{N_l} \sum_{j=1}^{N_w} \alpha \frac{\bar{k}_{m,i,j} V_{p,i,j}}{\bar{\phi}_{m,i,j} \mu_o L_{ij}^2} (p_{jm} - p_{im}) - \tau_{ijkmf} + q_{im} = \frac{dp_{im}}{dt} \sum_{k=1}^{N_l} C_{tk} V_{ikm} \quad (14)$$

$$\sum_{k=1}^{N_l} \sum_{j=1}^{N_w} \alpha \frac{\left[ 1 + \frac{b_k y_{ij}}{1 + c_k y_{ij}} (R_{k,\max} - 1) \right] \bar{k}_{f,i,j} V_{p,i,j}}{\bar{\phi}_{f,i,j} \mu_o L_{ij}^2} (p_{jf} - p_{if}) + \tau_{ijkmf} + q_{if} = \frac{dp_{if}}{dt} \sum_{k=1}^{N_l} C_{tk} V_{ikf} \quad (15)$$

where  $N_w$  is the number of wells connected to well  $I$ ,  $N_l$  is the number of reservoir layers, and  $q_{im}$  and  $q_{if}$  are the fluid flow rates of well  $i$  in the source and sink phases of the matrix and fracture systems under reservoir conditions, in  $\text{m}^3/\text{d}$ , respectively. If well  $i$  is a producing well, the fluid volume is positive; if it is an injection well, the fluid volume is negative.  $p_{im}$  and  $p_{jm}$  are the partial pressures of wells  $i$  and  $j$  in the matrix system, in MPa, respectively, with 7 and 8 as the partial pressures of wells  $i$  and  $j$  in the fracture system, in MPa, respectively;  $p_{if}$  and  $p_{jf}$  are the partial pressures of wells  $i$  and  $j$  in the fracture system, in MPa, respectively;  $\tau_{ijkmf}$  is the fracture flow rate between the matrix and the fracture systems between wells  $i$  and  $j$  in the  $k$ -th layer, in  $\text{m}^3/\text{d}$ ;  $C_{tk}$  is the integrated compression coefficient of the  $k$ -th layer, in  $\text{MPa}^{-1}$ ;  $V_{ikm}$  and  $V_{ikf}$  are the control volumes of well  $i$  in the matrix and in the fracture of the  $k$ -th layer, in  $\text{m}^3$ , respectively;  $\bar{k}_{m,i,j}$  and  $\bar{k}_{f,i,j}$  are the average permeability of the matrix and fracture, in mD.

The fugitive flow rate between the matrix and the fracture is calculated as follows:

$$\tau_{ijkmf} = \frac{\alpha K_m}{\mu} (p_{im} - p_{if}) \quad (16)$$

Pressure at time  $n$  can be obtained by using the above formula to calculate the pressure at time  $n-1$ . When the model operates under constant liquid production, the relationship between the pressure at time  $n$

and the pressure at time  $n-1$  is given by the following:

$$\begin{pmatrix} \omega_{1f}P_{1m}^{n-1} + \omega_{1m}P_{1f}^{n-1} \\ \omega_{2f}P_{2m}^{n-1} + \omega_{2m}P_{2f}^{n-1} \\ \vdots \\ \omega_{N_w f}P_{N_w m}^{n-1} + \omega_{N_w m}P_{N_w f}^{n-1} \end{pmatrix} = \begin{pmatrix} A_1 & -B_1(\eta_{12m}^n + \eta_{12f}^n) & \cdots & -B_1(\eta_{1N_w m}^n + \eta_{1N_w f}^n) \\ -B_2(\eta_{21m}^n + \eta_{21f}^n) & A_2 & \cdots & -B_2(\eta_{2N_w m}^n + \eta_{2N_w f}^n) \\ \vdots & \vdots & \cdots & \vdots \\ -B_{N_w}(\eta_{N_w 1m}^n + \eta_{N_w 1f}^n) & -B_{N_w}(\eta_{N_w 2m}^n + \eta_{N_w 2f}^n) & \cdots & A_{N_w} \end{pmatrix} \begin{pmatrix} P_{1f}^n \\ P_{2f}^n \\ \vdots \\ P_{N_w f}^n \end{pmatrix} + \begin{pmatrix} C_1 \\ C_2 \\ \vdots \\ C_{N_w} \end{pmatrix} \quad (17)$$

$$\omega_{im} = \frac{\Delta t^n}{\sum_{k=1}^{N_i} C_{tk} V_{ikm}^n}; \quad \omega_{if} = \frac{\Delta t^n}{\sum_{k=1}^{N_i} C_{tk} V_{ikf}^n}; \quad \eta_{ijm}^n = \sum_{k=1}^{N_i} T_{ijkm}^n; \quad \eta_{ijf}^n = \sum_{k=1}^{N_i} T_{ijkf}^n; \quad \varphi_{im} = \sum_{j=1}^{N_w} \eta_{ijm}^n; \quad \varphi_{if} = \sum_{j=1}^{N_w} \eta_{ijf}^n;$$

$$A_i = (\omega_{im} + \omega_{if}) + \omega_{im}\omega_{if}(\varphi_{im} + \varphi_{if}); \quad B_i = \omega_{im}\omega_{if}; \quad C_i = \omega_{im}\omega_{if} \left( \sum_{j=1}^{N_w} \eta_{ijf}^n \frac{\mu\tau_{ijkmf}^{n-1}}{\alpha K_m} - \frac{\mu\tau_{ijkmf}^{n-1}}{\alpha K_m} \varphi_{if} \right) - \omega_{im} \frac{\mu\tau_{ijkmf}^{n-1}}{\alpha K_m} - \omega_{im}\omega_{if}q_i^n$$

The Buckley–Leverett theory can be applied to track saturation after the completion of the pressure solution. The specific principles and calculation processes are detailed in the article by Zhao et al. [24]. As introduced in the previous section, corrections to the viscosity and relative permeability of the microgel solution are necessary, as shown in Eqs. (3) and (8). Then, the water content was calculated using the following formula:

$$f_w = 1 / \left( 1 + \frac{K_{rp}\mu_l}{K_{ro}\mu_o} \right) = 1 / \left( 1 + \frac{K_{rp}\mu_w(1 + ry_i + sy_i^2)}{K_{ro}\mu_o} \right) \quad (18)$$

A numerical simulation method for microgel flooding was developed based on the above theory and primarily consists of the following five steps:

1. The connectivity conductivity was calculated before microgel injection using the water-drive connectivity model.
2. The splitting factor of the injection well for each surrounding channel was calculated based on the flow rate of each channel.
3. The microgel solution concentration in each channel was calculated based on the critical splitting factor.
4. The absolute permeability reduction factor was calculated based on the concentration. The permeability of each channel was determined after microgel injection. Finally, the connectivity conductivity was corrected.
5. Production from each well is predicted based on the numerical simulation model.

#### 4 Calculus Analysis

A four-injection model was established to validate the accuracy of the model proposed in this study. The average pore sizes in the four directions were 14.08, 10.9, 6.2, and 3.4  $\mu\text{m}$ . The daily oil production rate for the oil wells was set at 10  $\text{m}^3$ , while the daily water injection rate for the water wells was set at 50  $\text{m}^3$ . After 1800

days of water flooding, a  $2.5 \text{ kg/m}^3$  microgel solution was injected. Following microgel injection, no microgel entered the smaller pore channels, as the partial flow rate was below the critical value of 0.1. However, the microgel concentration in the larger pore channels reached  $1.702 \text{ kg/m}^3$ , with a viscosity of  $1.0017 \text{ mPa}\cdot\text{s}$ . The permeability of the rock decreased to 93.8% of its initial value, and the flow distribution between channels became more uniform.

Fig. 1 shows a comparison of conductivity before and after microgel injection. A significant reduction in conductivity was observed between wells I1 and P1, with a 37% decrease following microgel treatment. Similarly, conductivity between wells I1 and P2 decreased by 35%. Notable changes in conductivity were also observed between other injection and production wells, particularly after microgel injection. These changes indicate that the swelling characteristics of microgels, along with their flexibility and high elasticity, facilitate the blocking of large pores while ensuring the smooth flow through small pores and achieving selective plugging.

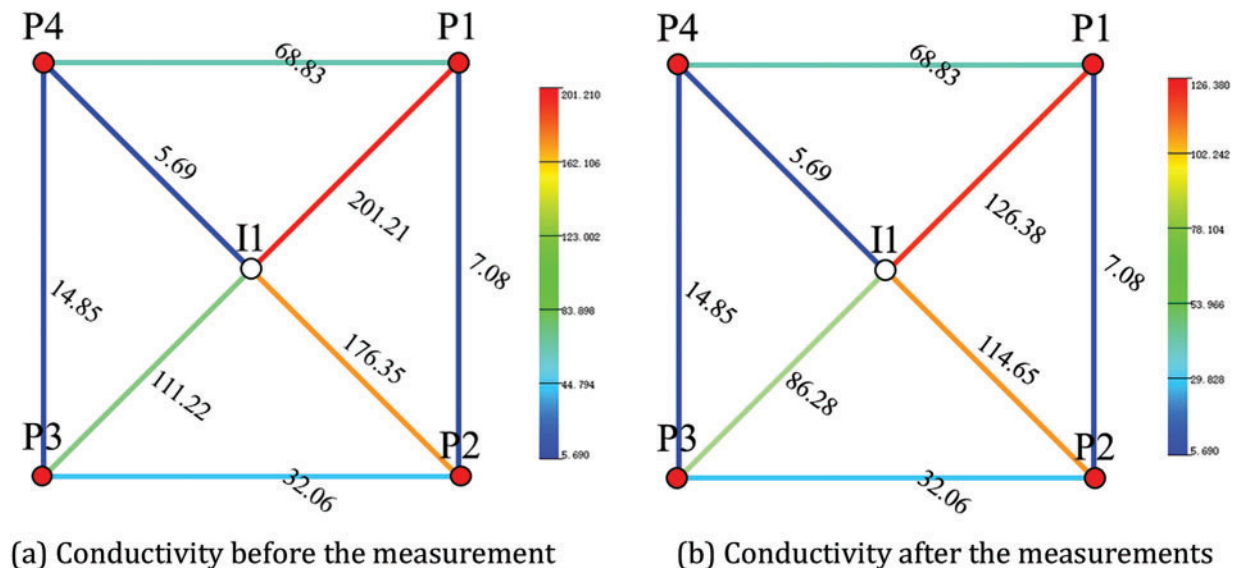


Figure 1: Conductivity comparison before and after the measures

The microgel selectively plugs high-permeability large pores, reduces cross-flow in the high-permeability zone, increases fluid kinetic energy in smaller pores, improves sweep efficiency, and enhances residual oil displacement. Additionally, the adjustable viscosity characteristics of the microgels effectively match the reservoir conditions, achieving better mobility control and enhancing oil displacement efficiency. This is ultimately reflected in the single-well productivity. The oil production rate of the block increased from  $3.93$  to  $5.04 \text{ m}^3/\text{d}$ , demonstrating an improvement of 28.24%. Specifically, the production of wells P1, P2, P3 and P4 increased from  $2.18$ ,  $0.92$ ,  $0.49$  and  $0.67 \text{ m}^3/\text{d}$  to  $2.52$ ,  $1.36$ ,  $0.69$  and  $0.85 \text{ m}^3/\text{d}$ , respectively, as shown in Fig. 2A–D).

## 5 Practical Block Applications

A complex medium-deep reservoir is characterized by a layered structure. In this study, the permeability distribution of the reservoir ranged from  $24.8$  to  $3721.4 \text{ mD}$ , with an average permeability of  $1079.8 \text{ mD}$ , indicating significant heterogeneity. The reservoir operates under normal temperature and pressure conditions, and the crude oil viscosity ranges from  $8.53$  to  $16.11 \text{ mPa}\cdot\text{s}$ . The reservoir contains three horizontal

wells, i.e., C07H, C08H, and C10H, with C08H serving as the water injection well and C07H and C10H serving as the production wells. The production commenced on 08 May 2014, and a total of 3006 production days have been achieved to date. After 1135 days of production, a 1-month microgel chemical profile control was conducted using a 2500-ppm microgel solution, which resulted in a noticeable increase in oil recovery during the later stages. To validate the numerical simulation method for microgel flooding proposed in this paper, a connectivity model of the reservoir was established to simulate the production of each well. The simulation results were compared with actual production data. The left side of Fig. 3 shows the connected conductivity field of the reservoir. It is worth noting that the repeated well names in the figure indicate that the horizontal well is equivalent to multiple nodes. The right side of Fig. 3 displays a comparison of the oil production rate of well A07H, where the blue curve and red circle represent the actual and simulated oil production rates, respectively. As shown in Fig. 3, the model demonstrates a good simulation performance, with a fitting rate close to 90%. After injecting the microgel solution, the simulation results closely followed the actual production trend, confirming the accuracy of the microgel flooding numerical simulation model proposed in this study.

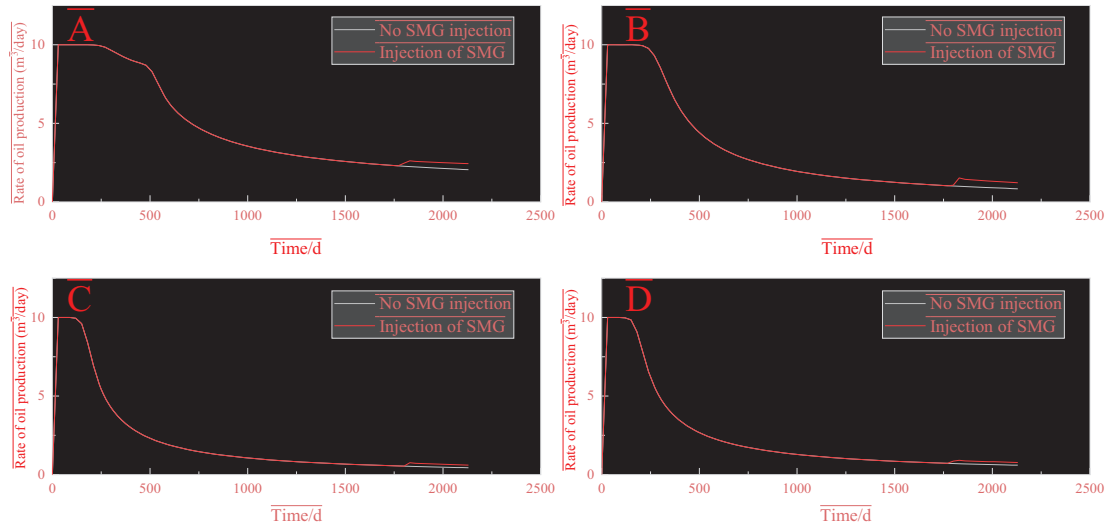


**Figure 2:** Oil production curves of the wells before and after plugging of P1 (A), P2 (B), P3 (C), and P4 (D)

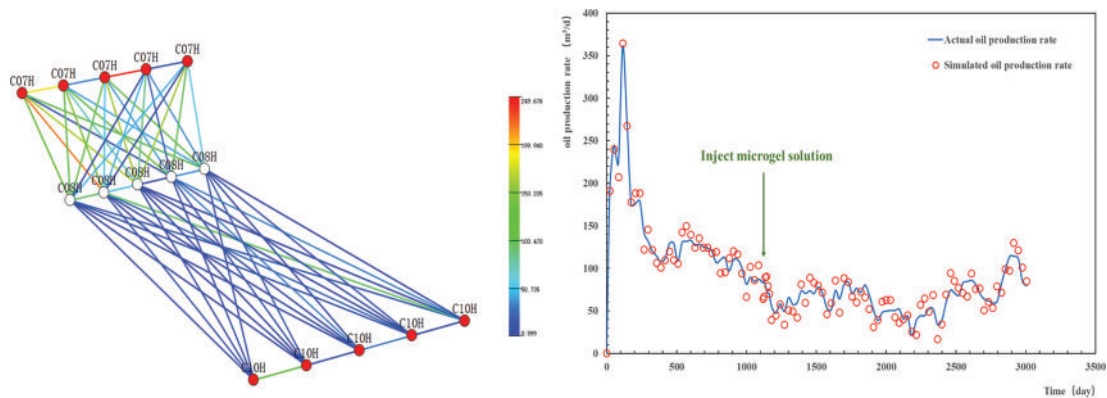


**Figure 3:** Connected conductivity field diagram of the reservoir and oil production rate of well A07H

## 6 Conclusion

(1) This paper introduces the oil displacement mechanism of a microgel chemical agent and quantitatively characterizes its fluid flow capacity.

(2) The solution viscosities at different pore scales is quantitatively characterized. A hybrid rheological framework was used to adjust the viscosity, considering the swelling behavior of microgels under varying shear rates and salinity conditions.

(3) Based on the dual-medium connectivity model, this study examines the impact of microgel flooding on the absolute and relative permeabilities of rock and fluid. A numerical simulation model for microgel chemical flooding was developed.

(4) The results from the conceptual example validation and real block application simulations demonstrate that the proposed connectivity model accurately reflects the microgel flooding mechanism, with the simulation outcomes fitting over 90% of the actual production data.

**Acknowledgement:** None.

**Funding Statement:** This study was supported by the National Natural Science Foundation project “Micro-Scale Effect of Oil-Gas Flow and the Mechanism of Enhancing Shale Oil Recovery by Natural Gas Injection” (No. 52074317).

**Author Contributions:** The authors confirm contribution to the paper as follows: Study Conception and Design: Tao Wang, Jie Gao, Xinlong Zhang; Literature Collection: Fei Wang, Hao Yang; Draft Manuscript Preparation: Guirong Di, Pengrun Wang; Manuscript Review and Supervision: Tao Wang, Haiyang Yu. All authors reviewed the results and approved the final version of the manuscript.

**Availability of Data and Materials:** All data generated or analyzed during this study are included in this published article.

**Ethics Approval:** Not applicable.

**Conflicts of Interest:** The authors declare no conflicts of interest to report regarding the present study.

## References

1. Xue L, Liu P, Zhang Y. Status and prospect of improved oil recovery technology of high water cut reservoirs. *Water*. 2023;15(7):1342. doi:10.3390/w15071342.
2. Ezeh O, Ikiensikimama SS, Akaranta O. Critical review of polymer flooding in Daqing field and pelican field: case studies of the world's largest polymer flooding in light and heavy oil reservoirs, respectively. *J Eng Res Rep*. 2021;21(10):25–40. doi:10.9734/jerr/2021/v21i1017497.
3. Sun G, Li P, Du D, Song T, Lu D. Numerical simulation of in-depth profile control for dispersed particle gel in heterogeneous reservoirs. *Front Energy Res*. 2023;11:1106191. doi:10.3389/fenrg.2023.1106191.
4. Kang WL, Zhou BB, Issakhov M, Gabdullin M. Advances in enhanced oil recovery technologies for low permeability reservoirs. *Petrol Sci*. 2022;19(4):1622–40. doi:10.1016/j.petsci.2022.06.010.
5. Yuan S, Han H, Wang H, Luo J, Wang Q, Lei Z, et al. Research progress and potential of new enhanced oil recovery methods in oilfield development. *Petrol Explor Dev*. 2024;51(4):963–80. doi:10.1016/S1876-3804(24)60518-5.
6. Temizel C, Canbaz CH, Palabiyik Y, Putra D, Asena A, Ranjith R, et al. A comprehensive review of smart/intelligent oilfield technologies and applications in the oil and gas industry. In: *SPE Middle East Oil and Gas Show and Conference*; 2019 Mar 18–21; Manama, Bahrain: SPE; 2019. doi:10.2118/195095-ms.
7. Seifi F, Haghightat F, Nikravesh H, Kazemzadeh Y, Azin R, Osfouri S. Using new chemical methods to control water production in oil reservoirs: comparison of mechanical and chemical methods. *J Petrol Explor Prod Technol*. 2024;14(10):2617–55. doi:10.1007/s13202-024-01844-1.

8. Tavakkoli O, Kamyab H, Shariati M, Mustafa Mohamed A, Junin R. Effect of nanoparticles on the performance of polymer/surfactant flooding for enhanced oil recovery: a review. *Fuel*. 2022;312:122867. doi:10.1016/j.fuel.2021.122867.
9. Seright RS, Wang D. Polymer flooding: current status and future directions. *Petrol Sci*. 2023;20(2):910–21. doi:10.1016/j.petsci.2023.02.002.
10. Lamas LF, Botechia VE, Schiozer DJ, Rocha ML, Delshad M. Application of polymer flooding in the revitalization of a mature heavy oil field. *J Petrol Sci Eng*. 2021;204:108695. doi:10.1016/j.petrol.2021.108695.
11. Amakiri KT, Canon AR, Molinari M, Angelis-Dimakis A. Review of oilfield produced water treatment technologies. *Chemosphere*. 2022;298:134064. doi:10.1016/j.chemosphere.2022.134064.
12. Zheng A, Feng Q, Wei Q, Liu D. Research on profile inversion pattern of polymer flooding. *Geosyst Eng*. 2018;21(3):135–41. doi:10.1080/12269328.2017.1382396.
13. Li J, Niu L, Wu W, Sun M. The reservoir adaptability and oil displacement mechanism of polymer microspheres. *Polymers*. 2020;12(4):885. doi:10.3390/polym12040885.
14. Lu X, Cao B, Xie K, Cao W, Liu Y, Zhang Y, et al. Enhanced oil recovery mechanisms of polymer flooding in a heterogeneous oil reservoir. *Petrol Explor Dev*. 2021;48(1):169–78. doi:10.1016/S1876-3804(21)60013-7.
15. Pahlevani H, Baghban Salehi M, Saghandali F, Moghanloo RG, Taghikhani V. Profile control and oil displacement in high temperature and salinity reservoirs: evaluation of deformable microgel system. *Polym Adv Technol*. 2024;35(8):e6530. doi:10.1002/pat.6530.
16. Abbas AH, Keldibayev N, Pourafshary P, Zhunisenkov Y, Serikov G. Numerical simulation of flaxseed gum potential in improving oil recovery: focus on offshore Kazakhstan. In: *Offshore Technology Conference Asia; 2024 Feb 27–Mar 1; Kuala Lumpur, Malaysia: OTC; 2024*. doi:10.4043/34861-ms.
17. Abbas AH, Abdullah DS, Jaafar MZ, Wan Sulaiman WR, Agi A. Comparative numerical study for polymer alternating gas (PAG) flooding in high permeability condition. *SN Appl Sci*. 2020;2(5):938. doi:10.1007/s42452-020-2673-8.
18. Hao H, Li J, Deng S, Xian B, Tang Z, Yang S, et al. N<sub>2</sub> foam flooding combined with gel plugging for enhanced oil recovery in high-temperature reservoirs: laboratory experiments and numerical simulations. *ACS Omega*. 2023;8(26):23913–24. doi:10.1021/acsomega.3c02383.
19. Zhao H, Kang Z, Zhang X, Sun H, Cao L, Reynolds AC. INSIM: a data-driven model for history matching and prediction for waterflooding monitoring and management with a field application. In: *SPE Reservoir Simulation Symposium; 2015; Houston, TX, USA: Society of Petroleum Engineers. SPE-173213-MS*. doi:10.2118/173213-ms.
20. Lee J, Koplík J. Network model for deep bed filtration. *Phys Fluids*. 2001;13(5):1076–86. doi:10.1063/1.1359747.
21. Sun Z, Wu X, Kang X, Lu X, Li Q, Jiang W, et al. Comparison of oil displacement mechanisms and performances between continuous and dispersed phase flooding agents. *Petrol Explor Dev*. 2019;46(1):121–9. doi:10.1016/S1876-3804(19)30011-4.
22. Thurston GB, Ozon PM, Pope GA. The viscoelasticity and gelation of some Polyacrylamide and xanthan gum solutions. In: *Proceedings of the American Institute of Chemical Engineers Spring National Meeting and Petro Expo; 1985; Houston, TX, USA*.
23. Abdelgawad KZ. Polymer induced permeability reduction: the influence of polymer retention and porous medium properties. *J Petrol Sci Eng*. 2022;217:110821. doi:10.1016/j.petrol.2022.110821.
24. Zhao H, Zhan W, Zhou Y, Zhang T, Li H, Rao X. A connection element method: both a new computational method and a physical data-driven framework—take subsurface two-phase flow as an example. *Eng Anal Bound Elem*. 2023;151:473–89. doi:10.1016/j.enganabound.2023.03.021.